Evidence of Complete Fusion in the Sub-Barrier $^{16}O + ^{238}U$ Reaction

K. Nishio,[1,*] H. Ikezoe,[1] Y. Nagame,[1] M. Asai,[1] K. Tsukada,[1] S. Mitsuoka,[1] K. Tsuruta,[1] K. Satou,[1] C. J. Lin,[1,†] and T. Ohsawa[2]

[1]*Japan Atomic Energy Research Institute, Tokai, Ibaraki 319-1195, Japan*

[2]*Department of Electrical & Electronic Engineering, School of Science & Engineering, Kinki University, Osaka 577-8502, Japan*

(Received 11 March 2004; published 13 October 2004)

Evaporation residue cross sections in the $^{16}O + ^{238}U$ reaction were measured for the energy range from above- to extreme sub-barrier. The cross sections are reproduced by a statistical model calculation, for which partial cross sections are calculated by a coupled-channel model taking into account the prolate deformation of ^{238}U. Complete fusion was observed in the collision of the projectile with the tips of the ^{238}U target, in the same way as the side collision.

DOI: 10.1103/PhysRevLett.93.162701 PACS numbers: 25.70.Jj, 24.60.Dr, 25.60.Pj, 27.90.+b

Recently, there has been much interest in the fission fragment angular distribution in sub-barrier heavy-ion reactions using actinide targets [1–8]. This is because of the observation that the angular anisotropies [$A = W(180°)/W(90°)$] in the sub-barrier region show much larger values than the prediction of the standard transition state model (TSM) [9]. In order to explain the anomalous behavior, two models are proposed. One is the fission before the K equilibrium and the other is the orientation dependent quasifission model.

The preequilibrium K-state model [10] implies that the fission takes place before the K degree of freedom is fully equilibrated. In the model of Ref. [6], the equilibrium of K distribution is not achieved for fusion-fission reactions with entrance channel mass-asymmetry smaller than the Businaro-Gallone mass-asymmetry [11] (for example $^{16}O + ^{238}U$). The increase of fragment anisotropy in the sub-barrier region is explained by the longer relaxation time of the K-degree of freedom. A static deformation of the target nucleus was taken into account in the entrance channel dependent K-state model [12]. This model succeeds to explain the effects of intrinsic spin of target [7] or projectile [8] on angular anisotropy.

For heavy-ion reactions with such energy as the fission barrier vanishes [13], the presence of quasifission is considered to be the reason for the large angular anisotropy. By assuming the quasifission to be dominated in the sub-barrier region, where the interaction of the projectile is restricted to the tips of the prolately deformed target, Hinde *et al.* [1] explained the energy dependence of the anisotropy for $^{16}O + ^{238}U$. The fusion-fission and quasifission was separated by the critical angle $35° \pm 5°$ defined by the incidence of the projectile to the symmetry axis of the target.

The presence (or absence) of complete fusion is unambiguously determined by measuring the evaporation residue (ER) cross section. For the $^{16}O + ^{238}U$ reaction, there have been two reports on the measurement of ER cross sections. The excitation functions are, however, quite different with each other. The maximum cross section for the $4n$ channel (^{250}Fm) appears at $E_{c.m.} = 80$ MeV in the data of Ref. [14], whereas the data in [15] gives the maximum at 86 MeV and the cross section drops below this energy. The different conclusions are derived in the sub-barrier region, necessitating further measurement.

In this Letter, we report on the measurement of ER cross sections for $^{16}O + ^{238}U$, and the excitation functions for $^{250\,249\,248}Fm$ (σ_{xn}, $x = 4, 5, 6$) are determined. Emphasis was put especially on the extreme sub-barrier energy region. We employed an aerosol-loaded He-gas-jet system to transport ERs, and their α decays are detected to determine the production rates. This method provides the efficient collection of ERs for the reaction like the present case, where the energy and angular distributions are broadly distributed after the ERs are recoiled out of the target.

The ^{16}O beams were supplied by the JAERI-tandem accelerator with the beam size of about 1 mm diameter. The natural uranium target was made by electrodeposition onto a Be-backing of 1.67 mg/cm^2 thickness with 5 mm diameter. The thickness was determined to be 320 μg/cm^2 by α spectrometry. The target included enriched ^{144}Sm material (~1 μg/cm^2) to produce α-decaying nucleus ^{156}Yb in the $^{16}O + ^{144}Sm$ reaction. This allowed us to check the stability of the transport efficiency of the gas-jet system. Before the electrodeposition, lead contained in the sample as impurity was removed by using an ion-exchange method in order to prevent the intense α-energy peak of ^{211m}Po, produced by the interaction with the beam, from overwhelming the α-energy spectra of Fm isotopes. The uniformity of the target thickness was checked by using a plastic detector; the tracks per 25×25 μm^2 on the detector, formed by α particles from the target being contacted with the surface of the detector, were uniformly distributed on the area corresponding to the electrodeposition face.

The beam passed through an window made of HAVAR foil (2.00 mg/cm^2), He cooling gas (0.09 mg/cm^2), Be

foil backing, and finally entered the target material. The reaction energy at the target was determined by calculating the energy loss in the foils and the cooling gas with the code TRIM [16]. The uncertainty of the bombarding energy was calculated to be $\sigma = 0.3$ MeV. This arises from (1) the straggling in the window and Be backing and (2) the variation of the bombarding energy resulting from the finite target thickness. The beam dose was determined by monitoring the beam current, and the typical beam current was 30–100 pnA.

The ERs recoiling out of the target were stopped in He-gas (97 kPa) loaded with KCl aerosol clusters. The ERs attached to the clusters were continuously swept out of the target chamber with a He-gas flow (2.0 l/ min), and transported through a Teflon capillary to a rotating wheel apparatus MAMON [17]. The transported nuclei were deposited on a polyester catcher foil (120 μg/cm^2) stretched on the periphery of the 80-cm-diameter wheel. The wheel having totally 80 catcher foils was rotated every 150 s to collect a new deposit. The α particles from the deposit were detected by a series of 18 silicon PIN photodiodes (18×18 mm^2). Accordingly, the maximum life measurable in the detector array is 45 min, which allows us to draw the decay curve of ^{250}Fm ($T_{1/2} =$ 30 min [18]). The single PIN photodiode was viewed by the deposition at a geometrical efficiency of 34%. In the data acquisition, we recorded a timing signal every 1 s in order to draw the decay curves of ^{248}Fm (36 s) and ^{249}Fm (2.6 min). The energy calibration of the photodiode was carried out by referring the known α energies of ^{208}Fr (6641 keV) and ^{204}At (5951 keV) produced by bombarding the ^{16}O-beams on the Au target (356 μg/cm^2). This reaction was also used to determine the transport efficiency for the ERs. Behind the target, a catcher foil (Al) was placed to collect ERs. The α decay of ^{204}At ($T_{1/2} =$ 9.2 min), the daughter of ^{208}Fr(59 s) produced in the reaction, was detected in a silicon detector mounted on a separate chamber to determine the production yield. By comparing the yield to the one at the polyester foil on the rotating wheel, we obtained the transport efficiency of 0.369 ± 0.019 at 36 pnA. The effect of the range of ERs in the He-gas cell on the transport efficiency was examined. The range was changed by depositing an aluminum layer as a degrader on the gold target. We found no significant difference in transport efficiencies.

Figure 1 shows the α-particle energy spectra for three selected reaction energies in the center-of-mass frame ($E_{\text{c.m.}}$) obtained from 18 photodiodes. The energy resolution is about 60 keV (FWHM). The α-particle energies for ^{250}Fm and ^{249}Fm agree with the literature values of 7430 and 7527 keV, respectively. The ^{248}Fm peak should contain two lines of 7870 keV (80%) and 7830 keV (20%), which are not distinguished in the spectrum because of the limited resolution. At the energy of 91.0 MeV, evaporation residues for ^{250}Fm, ^{249}Fm, and ^{248}Fm are observed. In the extreme sub-barrier energy of 73.5 MeV, the ^{250}Fm peak is still clearly observed. It should be mentioned that this energy corresponds to the interaction energy of ^{16}O to the tips of the deformed ^{238}U target.

The decay curves of three Fm isotopes are shown in Fig. 2. They are obtained by selecting the events constituting the specific energy peaks and by summing all the data taken in the measurement. The obtained half-life ($T_{1/2}$) for ^{248}Fm 31.6 ± 4.2 s is close to the literature value 36 s [18]. Our data of 20.1 ± 8.0 min for ^{250}Fm are smaller than 30 min in [18]. The $T_{1/2}$ for ^{249}Fm also shows smaller value 1.95 ± 0.25 than 2.6 min [18].

The cross sections for three Fm isotopes obtained in this work are shown in the upper part of Fig. 3. The errors show the statistical error. In the analysis, the branching ratio of the α decay was used as 0.95 (^{250}Fm), 0.15 (^{249}Fm), and 0.99 (^{248}Fm) [18]. Our data are close to those of [14] in the absolute values and the $E_{\text{c.m.}}$ values corresponding to the maximum cross sections for each xn channels. The $4n$-channel cross section in Ref. [15] is

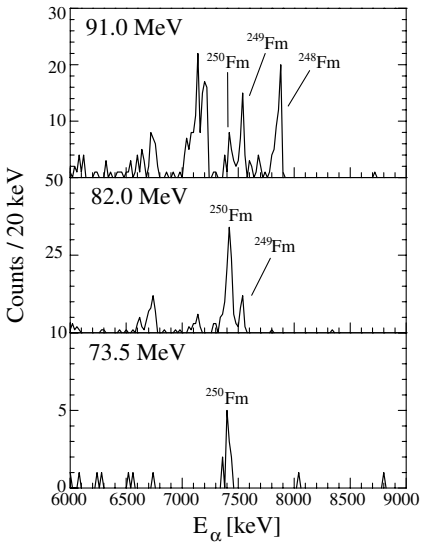

FIG. 1. Energy spectra of α particles for $E_{\text{c.m.}}$ indicated.

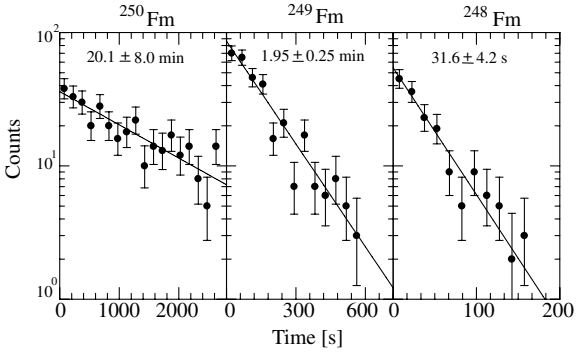

FIG. 2. Decay curves of α activities for fermium isotopes.

about 4 times larger at the maximum than the present data and the peak energy is about 7 MeV larger.

In order to consider the fusion process in the sub-barrier energy region, a statistical model calculation was carried out by using the code HIVAP [19]. The calculation needs the partial wave cross section for angular momentum L, $\sigma(L)$, for the fusion process, which varies largely from that of the one-dimensional model at and below the Coulomb barrier as the results of coupling between the relative motion and several nuclear collective motions. The $\sigma(L)$ and fusion cross section $\sigma_{\rm fus}$ are calculated by the coupled-channel code CCDEGEN [20], which is based on a version of the CCFULL code described in [21]. To take into account the effects of target deformation on the fusion process, the CCDEGEN code determines the tunneling probability for partial wave L, $P_L(E_{\rm c.m.}, \theta)$, for a given colliding angle θ of the projectile with respect to the symmetric axis of the target. The total tunneling probability $P_L(E_{\rm c.m.})$ is thus calculated by taking the average over all orientations as

$$P_L(E_{\rm c.m.}) = \frac{1}{2}\int_0^{\pi} P_L(E_{\rm c.m.}, \theta)\sin\theta d\theta.$$

Because of the highly fissile compound nucleus ^{254}Fm formed in the present reaction, the fusion cross section is well approximated to the fission cross section, in so far as the system fuses completely. The thin solid curve in the upper part of Fig. 3 represents the fusion cross section calculated by the CCDEGEN code. We adopted the quadruple and hexadecapole deformation parameters of $(\beta_2, \beta_4) = (0.275, 0.05)$ for ^{238}U as in Ref. [1]. Up to two phonon states are included for the octupole vibration in ^{238}U with the first excitation energy 0.73 MeV [18], and the deformation parameter β_3 of 0.086 [22] was used.

The calculation reproduces the fission cross sections of Ref. [1] shown by the open circles. In the highest energy region of $E_{\rm c.m.} > 95$ MeV, we can find the agreement with the fission cross section of Ref. [23]. For comparison, we show the calculation ignoring the deformation of ^{238}U and couplings to the collective states (dotted curve). This one-dimensional model sharply drops below the Coulomb barrier $V_{\rm B} = 81.4$ MeV. The lower part of Fig. 3 shows the barrier distribution $D(E_{\rm c.m.})$ defined by the second derivative of the function $E_{\rm c.m.}\sigma_{\rm fus}$ with respect to energy [24]. The coupled-channel calculation (solid curve) reproduces the global shape of the measured barrier distribution [1] that the left wing grows to the lowest energy as the results of prolate deformation of ^{238}U. The lowest fusion barriers are associated with collisions of the ^{16}O with the tips of ^{238}U, while the highest barriers corresponds to the collisions with the side. The calculation overestimates the experimental barrier distribution around $E_{\rm c.m.} = 83$ MeV. However, this does not alter our discussions especially on the sub-barrier fusion process.

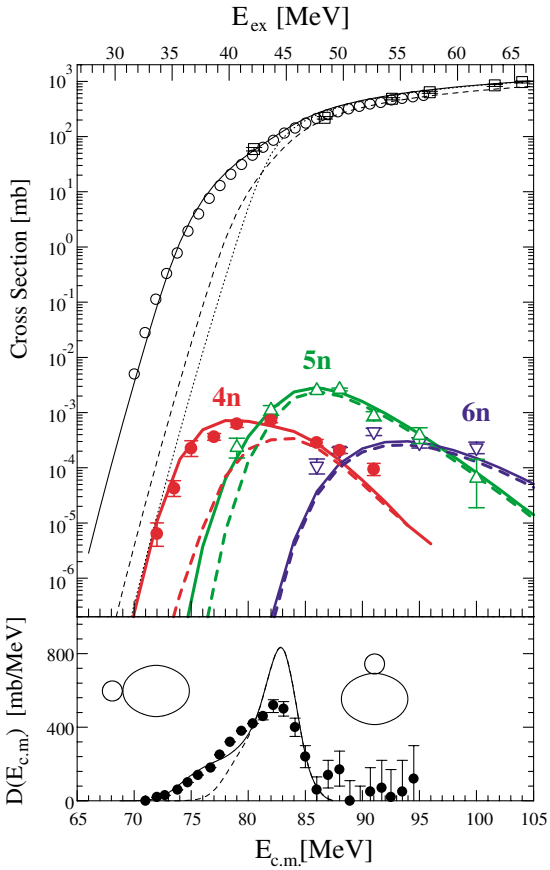

FIG. 3 (color). (Upper part) Evaporation residue cross sections for ^{250}Fm (solid circles), ^{229}Fm (open triangles), and ^{248}Fm (reversed triangles) in the ^{16}O + ^{238}U reaction. The fusion cross sections from the CCDEGEN code (thin solid curve) taking into account the deformation of ^{238}U and couplings to the octupole phonon states in ^{238}U are compared to the fission cross section from Refs. [1] (open circles) and [23] (open squares). The bold solid curves are the calculated ER cross sections. The thin dotted curve is the fusion cross section without any couplings. The thin dashed curve is the fusion cross section assuming the fusion hindrance in the tip collisions, and the corresponding ER cross sections are shown by bold dashed curves. (Lower part) Barrier distributions in Ref. [1] are compared to those from the coupled-channel calculation (solid curve). Two touching configurations corresponding to low and high interaction energies are illustrated. The dashed curve represents the barrier distribution which assumes the fusion hindrance in the tip collisions.

The partial wave cross sections from the CCDEGEN code were used as input to the HIVAP code to calculate the ER cross sections. The results are shown by thick curves for three Fm isotopes. In the calculation, we modified the parameter $b_{\rm fac}$ slightly, which is multiplied to the fission barrier height of the liquid-drop part [25], so as to obtain the agreement with the experimental data in the above-barrier region. In the sub-barrier region, the calculation also reproduced the cross sections for ^{250}Fm. This indicates that the collision of the projectile with the

tips of ^{238}U also results in complete fusion without any significant fusion hindrance.

We tried to calculate the ER cross sections within the constraint that the collision of the projectile with the tips of ^{238}U does not form the compound nucleus as is discussed in Ref. [1]. The tunneling probability $P_L(E_{\mathrm{c.m.}}, \theta)$ is set to be zero for the interactions of $0° \leq \theta < 30°$. The corresponding fusion cross sections are shown by the thin dashed curve in Fig. 3. Below $E_{\mathrm{c.m.}} = 78$ MeV being the Coulomb potential at $\theta = 30°$, the fusion cross section falls sharply and the barriers $D(E_{\mathrm{c.m.}})$ in the lowest energy region disappear. The resulting ER cross sections are shown by bold dashed curves. Fermium 248 ($6n$ channel) is predominantly produced in the above-barrier region and the cross section is missing only the geometrical fraction corresponding the tip collisions (13%), so that the agreement between the calculation and the experimental data is still preserved. This is the case for the cross sections of ^{250}Fm ($4n$ channel) in the above-barrier region. On the contrary, in the extreme sub-barrier region, the calculation considering the fusion hindrance is about 2 orders of magnitude smaller than the experimental data.

We conclude that in the sub-barrier region, complete fusion is the main process after the projectile is captured to the target, and the orientation dependent quasifission is not the reason for the anomalously large fission fragment angular anisotropy. The fission events in the sub-barrier region are ascribed to fusion-fission rather than quasifission. The preequilibrium K-state model at the saddle configuration seems to be an account for the anomalous behavior of the angular anisotropy. Another idea to explain this phenomenon is the one by Freifelder *et al.* [26] that the deformation in the fission process is slow enough to allow for the statistical K equilibrium even for configurations well beyond the saddle point.

The present result for the ^{16}O + ^{238}U reaction is at variance with our recent measurements [27] using a deformed target, in which quasifission dominates in the sub-barrier region for ^{76}Ge + ^{150}Nd and ^{60,64}Ni + ^{154}Sm. The inconsistency is explained qualitatively by the Z_pZ_t value (proton number of projectile and target). The systematics in [28] shows that the reaction larger than $Z_pZ_t \simeq 1800$ shows fusion hindrance at the Coulomb barrier. The fusion hindrance is defined by the "extra-extra-push energy," which is an additional kinetic energy over the Coulomb barrier needed for a system to achieve complete fusion [29]. For ^{16}O + ^{238}U ($Z_pZ_t = 736$), the light ^{16}O nucleus is easily captured by the target for every colliding angle. This is not the case for ^{76}Ge + ^{150}Nd (1920) and ^{60,64}Ni + ^{154}Sm (1736), where the massive projectile does not fuse for the tip collisions but fuses for the side collisions.

The authors thank the crew of the JAERI-tandem facility for the beam operation. Thanks are due to Dr. Hagino of Kyoto University for fruitful discussions.

*Electronic address: nishio@popsvr.tokai.jaeri.go.jp
†On leave from China Institute of Atomic Energy, Beijing 102413, China

[1] D. J. Hinde *et al.*, Phys. Rev. Lett. **74**, 1295 (1995).
[2] J. C. Mein *et al.*, Phys. Rev. C **55**, 995(R) (1997).
[3] H. Zhang *et al.*, Phys. Rev. C **49**, 926 (1994).
[4] N. Majumdar *et al.*, Phys. Rev. C **51**, 3109 (1995).
[5] A. Karnik *et al.*, Z. Phys. A **351**, 195 (1995).
[6] Z. Liu *et al.*, Phys. Lett. B **353**, 173 (1995).
[7] J. P. Lestone *et al.*, Phys. Rev. C **56**, 2907(R) (1997).
[8] B. K. Nayak *et al.*, Phys. Rev. C **62**, 031601(R) (2000).
[9] R. Vandenbosch and J. R. Huizenga, *Nuclear Fisson* (Academic Press, New York, 1973).
[10] V. S. Ramamurthy and S. S. Kapoor, Phys. Rev. Lett. **54**, 178 (1985).
[11] U. L. Businaro and S. Gallone, Nuovo Cimento **5**, 315 (1957); K. Thomas, R. Davies, and A. J. Sierk, Phys. Rev. C **31**, 915 (1985).
[12] D. Vorkapic and B. Ivanisevic, Phys. Rev. C **52**, 1980 (1995).
[13] B. B. Back *et al.*, Phys. Rev. C **32**, 195 (1985).
[14] G. N. Akap'ev *et al.*, Sov. J. At. En. **21**, 908 (1966).
[15] N. Shinohara *et al.*, Phys. Rev. C **34**, 909 (1986).
[16] J. F. Ziegler, J. P. Biersack, and U. Littmark, *The Stopping and Range of Ions in Solids* (Pergamon, New York, 1985).
[17] Y. Nagame *et al.*, J. Nucl. Radiochem. Sci. **3**, 85 (2002).
[18] R. B. Firestone, *Table of Isotopes*, edited by V. S. Shirley (Wiley, New York, 1996).
[19] W. Reisdorf and M. Schädel, Z. Phys. A **343**, 47 (1992).
[20] K. Hagino (unpublished).
[21] K. Hagino, N. Rowley, and A. T. Kruppa, Comput. Phys. Commun. **123**, 143 (1999).
[22] R. H. Spear, At. Data Nucl. Data Tables **42**, 55 (1989).
[23] V. E. Viola and T. Sikkeland, Phys. Rev. **128**, 767 (1962).
[24] N. Rowley, G. R. Satchler, and P. H. Stelson, Phys. Lett. B **254**, 25 (1991).
[25] S. Cohen, F. Plasil, and W. J. Swiatecki, Ann. Phys. (N.Y.) **82**, 557 (1974).
[26] R. Freifelder *et al.*, Phys. Rep. **133**, 315 (1986).
[27] K. Nishio *et al.*, Phys. Rev. C **62**, 014602 (2000); S. Mitsuoka *et al.*, Phys. Rev. C **62**, 054603 (2000); K. Nishio *et al.*, Phys. Rev. C **63**, 044610 (2001); S. Mitsuoka *et al.*, Phys. Rev. C **65**, 054608 (2002).
[28] A B. Quint *et al.*, Z. Phys. A **346**, 119 (1993).
[29] W. J. Swiatecki, Nucl. Phys. **A376**, 275 (1982); S. Bjørnholm and W. J. Swiatecki, Nucl. Phys. **A391**, 471 (1982).